Regulation of membrane scission in yeast endocytosis

Deepikaa Menon, Daniel Hummel, and Marko Kaksonen*
Department of Biochemistry and National Centre of Competence in Research, Chemical Biology, University of Geneva, CH-1211 Geneva Switzerland

ABSTRACT **During clathrin-mediated endocytosis, a flat plasma membrane is shaped into an invagination that undergoes scission to form a vesicle. In mammalian cells, the force that drives the transition from invagination to vesicle is primarily provided by the GTPase dynamin that acts in concert with crescent-shaped BAR domain proteins. In yeast cells, the mechanism of endocytic scission is unclear. The yeast BAR domain protein complex Rvs161/167 (Rvs) nevertheless plays an important role in this process: deletion of Rvs dramatically reduces scission efficiency. A mechanistic understanding of the influence of Rvs on scission, however, remains incomplete. We used quantitative live-cell imaging and genetic manipulation to understand the recruitment and function of Rvs and other late-stage proteins at yeast endocytic sites. We found that arrival of Rvs at endocytic sites is timed by interaction of its BAR domain with specific membrane curvature. A second domain of Rvs167—the SH3 domain—affects localization efficiency of Rvs. We show that Myo3, one of the two type-I myosins in *Saccharomyces cerevisiae*, has a role in recruiting Rvs167 via the SH3 domain. Removal of the SH3 domain also affects assembly and disassembly of actin and impedes membrane invagination. Our results indicate that both BAR and SH3 domains are important for the role of Rvs as a regulator of scission. We tested other proteins implicated in vesicle formation in *S. cerevisiae* and found that neither synaptojanins nor dynamin contribute directly to membrane scission. We propose that recruitment of Rvs BAR domains delays scission and allows invaginations to grow by stabilizing them. We also propose that vesicle formation is dependent on the force exerted by the actin network.**

Monitoring Editor
Patricia Bassereau
Institut Curie

Received: Jul 9, 2021
Revised: Jun 8, 2022
Accepted: Aug 8, 2022

INTRODUCTION

Clathrin-mediated endocytosis is a process by which cargo molecules from the cell exterior are incorporated into a clathrin-coated vesicle that is then transported into the cell. More than 50 different proteins are involved in formation of an endocytic vesicle (McMahon and Boucrot, 2011; Kaksonen and Roux, 2018). The molecular mechanisms mediating endocytic vesicle formation are largely conserved between yeast and mammals. Most yeast endocytic proteins have homologues in mammals. These proteins establish endocytic sites, recruit cargo, bend the membrane into an invagination, and finally separate the endocytic vesicle from the plasma membrane (Kaksonen and Roux, 2018). Actin filaments play a critical role in membrane shaping in yeast. The filaments are nucleated and polymerize to form a branched actin network, which is required for bending the membrane into stereotypical tubular invaginations (Kübler *et al.*, 1993; Kukulski *et al.*, 2012). How the final stage of membrane scission is effected in yeast remains unclear. In mammalian cells, the forces that drive the final transition from invagination to spherical vesicle are largely provided by the GTPase dynamin (Grigliatti *et al.*, 1973; Takei *et al.*, 1995; Sweitzer and Hinshaw, 1998; Ferguson *et al.*, 2007; Galli *et al.*, 2017). Dynamin interacts via its proline-rich domain with the SH3 domains of crescent-shaped N-BAR proteins like endophilin and amphiphysin (Grabs *et al.*, 1997; Cestra *et al.*, 1999; Farsad *et al.*, 2001; Ferguson *et al.*, 2009; Meinecke *et al.*, 2013). Conformational changes of dynamin

This article was published online ahead of print in MBoC in Press (http://www.molbiolcell.org/cgi/doi/10.1091/mbc.E21-07-0346) on August 17, 2022.

*Address correspondence to: Marko Kaksonen (Marko.Kaksonen@unige.ch).

Abbreviations used: CLEM, correlative light and electron microscopy; GPA, glycine proline alanine; PI(4,5)P_2, phosphatidylinositol 4,5-bisphosphate; Rvs, heterodimeric complex composed of Rvs167 and Rvs161; SH3, Src homology 3.

recruited to N-BAR molecules cause constriction of the underlying invaginated membrane, resulting in vesicle formation (Shupliakov *et al.*, 1997; Zhang and Hinshaw, 2001; Zhao *et al.*, 2016).

Three dynamin-like proteins, Dnm1, Mgm1, and Vps1, have been identified in yeast. Dnm1 and Mgm1 are involved in mitochondrial fusion and fission (Cerveny *et al.*, 2007). The third, Vps1, gets its name from its essential role in vacuolar protein sorting in the secretory pathway (Rothman *et al.*, 1989, 1990). It is also involved in fission and fusion of vacuoles and peroxisomes (Hoepfner *et al.*, 2001; Peters *et al.*, 2004) and is required for regulation of endosome-to-Golgi trafficking (Gurunathan *et al.*, 2002). In addition, Vps1 has been reported to localize at endocytic sites on the plasma membrane, interact with endocytic proteins like clathrin, and influence the lifetimes and recruitment of endocytic proteins (Yu and Cai, 2004; Nannapaneni *et al.*, 2010; Smaczynska-de Rooij *et al.*, 2012). Others, however, have failed to observe Vps1 at endocytic sites (Kishimoto *et al.*, 2011; Gadila *et al.*, 2017) or establish a role for Vps1 in endocytic vesicle scission (Nothwehr *et al.*, 1995; Kaksonen *et al.*, 2005). The role of Vps1 in clathrin-mediated endocytosis thus remains debated.

A confirmed component of the yeast endocytic scission mechanism is the heterodimeric complex formed by the N-BAR domain proteins Rvs161 and Rvs167 (Munn *et al.*, 1995; D'Hondt *et al.*, 2000; Kaksonen *et al.*, 2005; Kishimoto *et al.*, 2011). The two Rvs proteins are homologues of the N-BAR proteins amphiphysin and endophilin in animals (Friesen *et al.*, 2006; Youn *et al.*, 2010). Deletion of Rvs167 reduces scission efficiency by nearly 30% and reduces the lengths to which endocytic invaginations grow by nearly two thirds (Kaksonen *et al.*, 2005; Kukulski *et al.*, 2012). In endocytic events that fail to undergo scission, the membrane first invaginates and then retracts back to the cell wall (Kaksonen *et al.*, 2005). Rvs167 and Rvs161 proteins form a canonical N-BAR domain that forms a crescent-shaped structure (Youn *et al.*, 2010). This curved structure is thought to be the key functional domain of the protein (Sivadon *et al.*, 1997). N-BAR domains are able to form lattices that can bind membrane with their concave surfaces and impose or sense curvature across dimensions larger than that of a single BAR domain (Farsad *et al.*, 2001; Peter *et al.*, 2004; Youn *et al.*, 2010; Mim *et al.*, 2012; Zhao *et al.*, 2013). In addition to the N-BAR domain, Rvs167 has a glycine-proline-alanine–rich (GPA) region and a C-terminal SH3 domain (Sivadon *et al.*, 1997). The GPA region is thought to act as a linker with no other known function, while the SH3 domain affects daughter cell budding and actin cytoskeleton morphology (Sivadon *et al.*, 1997). The Rvs complex can tubulate liposomes in vitro, indicating that the Rvs BAR domain can impose curvature on membranes (Youn *et al.*, 2010). However, Rvs arrives at endocytic sites when membrane tubes are already formed (Kukulski *et al.*, 2012; Picco *et al.*, 2015). Therefore curvature-sensing rather than curvature-generation is the likely role of the Rvs complex at endocytic sites. Rvs molecules arrive at endocytic sites a few seconds before scission and disassemble rapidly at scission time (Picco *et al.*, 2015), consistent with a role in vesicle scission. However, a mechanistic understanding of the role of Rvs in scission remains incomplete.

Synaptojanins are phosphatidylinositol 4,5-bisphosphate (PI(4,5)P_2) phosphatases that have been implicated in endocytic scission, as well as in intracellular signaling and modulation of the actin cytoskeleton (Singer-Krüger *et al.*, 1998). They interact with both dynamin and N-BAR proteins in mammalian cells (McPherson *et al.*, 1996; Watanabe *et al.*, 2018). Disruption of these genes leads to accumulation of PI(4,5)P_2 in yeast cells (Stolz *et al.*, 1998b). In synaptojain-disrupted mouse cells, coated endocytic vesicles cluster at the plasma membrane, demonstrating a role for lipid hydrolysis in vesicle uncoating (Watanabe *et al.*, 2018). In yeast, removal of synaptojanin-like proteins affects the rate of endocytosis and induces the aberrant behavior of several endocytic proteins (Singer-Krüger *et al.*, 1998; Sun *et al.*, 2007; Kishimoto *et al.*, 2011).

We aimed to identify roles and molecular mechanisms for proteins that have been implicated in endocytic vesicle scission in yeast: Vps1, synaptojanins, and the Rvs complex. We used quantitative live-cell imaging and genetic manipulation in *Saccharomyces cerevisiae* to test the roles of these proteins in endocytosis. We found evidence for a specific role in scission for the Rvs complex, but not for the other candidate proteins. Furthermore, we analyzed the molecular mechanisms of recruitment and the mode of action of Rvs in scission.

RESULTS

Rvs167, but not Vps1, influences endocytic coat internalization

The role of the dynamin-like protein Vps1 in yeast endocytosis is unclear. Some studies have reported a role for Vps1 in endocytic vesicle scission (Yu and Cai, 2004; Nannapaneni *et al.*, 2010; Smaczynska-de Rooij *et al.*, 2010), while others have reported that Vps1 does not localize to endocytic sites or contribute to scission (Kishimoto *et al.*, 2011; Gadila *et al.*, 2017). Neither N- nor C-terminally tagged Vps1 colocalized with endocytic actin-binding protein Abp1 in our hands (unpublished data), consistent with other work that observed localization only with the Golgi trafficking pathway (Gadila *et al.*, 2017). However, the question of whether or not Vps1 has a function at endocytic sites has been obfuscated by potential tagging-induced dysfunction of Vps1 molecules.

In mammalian cells, dynamin interacts with N-BAR proteins to cause vesicle scission (Grabs *et al.*, 1997; Cestra *et al.*, 1999; Farsad *et al.*, 2001; Meinecke *et al.*, 2013). Although the association between yeast dynamin Vps1 and N-BAR protein Rvs is uncertain, Rvs is recruited to endocytic sites briefly before scission and influences scission efficiency (Kaksonen *et al.*, 2003, 2005; Kukulski *et al.*, 2012; Picco *et al.*, 2015). To determine the roles of these proteins in endocytic scission, we analyzed the behavior of other endocytic proteins in cells lacking Vps1 and Rvs167 and compared it against that of wild-type (WT) cells (Figure 1, A–F).

Vps1 gene deletion was confirmed by sequencing the gene locus. *vps1*Δ cells showed a previously reported slow-growth phenotype at high temperatures (Supplemental Figure S1A) (Rothman and Stevens, 1986). To quantify invagination progression, coat protein Sla1 tagged at the C-terminus with eGFP was observed in yeast cells imaged at the equatorial plane (Figure 1A). Because membrane invagination progresses perpendicularly to the plane of the plasma membrane, proteins that move into the cytoplasm during invagination growth do so in the imaging plane. Upon actin polymerization, the endocytic coat moves into the cytoplasm along with the membrane as it invaginates (Skruzny *et al.*, 2012). Movement of Sla1 thus acts as a proxy for the growth of the plasma membrane invagination. Membrane retraction, that is, inward movement and subsequent retraction of the invaginated membrane back toward the cell wall is a scission-specific phenotype (Kaksonen *et al.*, 2005; Kishimoto *et al.*, 2011). Retraction rates were not significantly different in *vps1*Δ cells compared to the WT cells (Figure 1B).

To follow invaginations in more detail, centroids of 30–50 Sla1-eGFP patches in *vps1*Δ and WT cells were tracked through time-lapse movies (Figure 1, A–C). These centroid trajectories of Sla1 patches—each patch being an endocytic site—were then aligned to each other and averaged to provide an averaged centroid that could be followed with high spatial and temporal precision

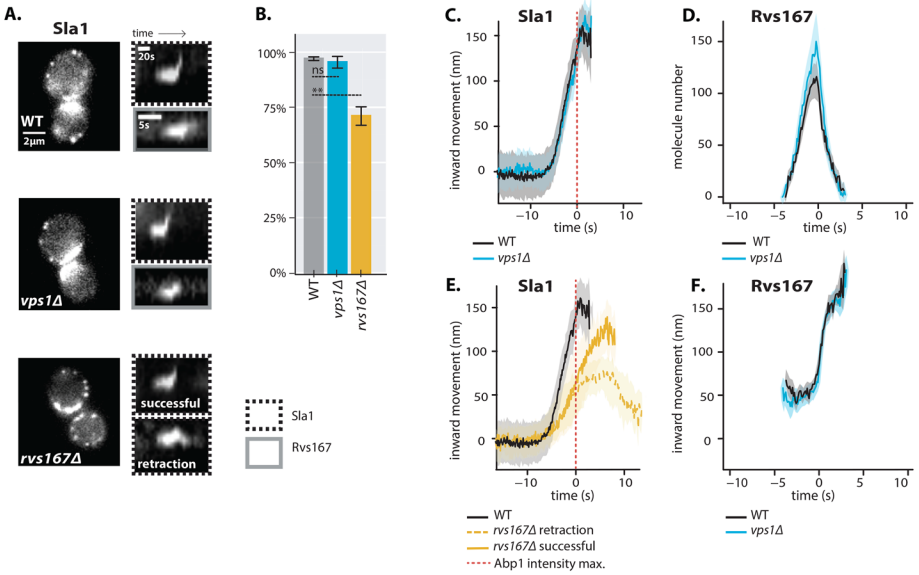

FIGURE 1: *rvs167*Δ but not *vps1*Δ changes coat movement. (A) Left: One thousand millisecond exposures from time-lapse movies of WT, *vps1*Δ, and *rvs167*Δ cells with endogenously tagged Sla1-eGFP. Right: Kymographs of Sla1-eGFP or Rvs167-eGFP in WT, *vps1*Δ, and *rvs167*Δ cells. (B) Scission efficiency in WT, *vps1*Δ, and *rvs167*Δ cells. Error bars are SD, *p* values from two-sided *t* test, $*p \leq 0.05$, $**p \leq 0.01$, $***p \leq 0.001$. (C) Average centroid positions of Sla1-eGFP in WT and *vps1*Δ cells. (D) Number of Rvs167 molecules in WT and *vps1*Δ cells. (E) Average centroid positions of Sla1-eGFP in WT and successful and retracted Sla1-eGFP positions in *rvs167*Δ cells. (F) Average centroid positions of Rvs167-eGFP in WT and *vps1*Δ cells. All centroids were coaligned with Abp1-mCherry so that time = 0 s corresponds to Abp1 intensity maximum and *y* = 0 nm corresponds to nonmotile positions of Sla1 in the respective strains. Shading on plots shows 95% confidence intervals. Dashed red lines indicate Abp1 intensity maxima in respective strains.

(Picco *et al.*, 2015). Sla1-eGFP was imaged simultaneously with Abp1-mCherry. Abp1 fluorescence intensity maximum in WT cells correlates with scission time and maximum movement of the Sla1 centroid (Supplemental Figure S1B) (Picco *et al.*, 2015). The movement of the Sla1-eGFP centroid therefore corresponds to the growth of the endocytic membrane invagination and to the initial diffusive movement of the vesicle after scission (Kukulski *et al.*, 2012; Picco *et al.*, 2015). The distance that the Sla1 centroid moves thus gives an indication of invagination and scission steps of endocytosis. Any defects in scission are expected to change the motility pattern of the Sla1 centroid.

The movement of Sla1-eGFP in WT cells was linear to about 150 nm (Figure 1C), consonant with maximum invagination lengths measured by correlative light and electron microscopy (CLEM) (Kukulski *et al.*, 2012). Sla1 movement in *vps1*Δ cells, also coaligned with Abp1-mCherry, was virtually identical to that in WT cells (Figure 1C). The total movement—and so the length of endocytic invagination—was similar to that of WT.

Quantitative imaging has shown that scission is simultaneous with a sharp jump of the Rvs167 centroid into the cytoplasm and a corresponding loss of fluorescence intensity (Figure 1, D and F, and Supplemental Figure S1B) (Kukulski *et al.*, 2012; Picco *et al.*, 2015). This jump is interpreted as loss of protein on the membrane tube at the time of scission, causing an apparent jump of the Rvs167 centroid to proteins that remain localized on the newly formed vesicle. Kymographs of Rvs167-GFP (Figure 1A), as well as Rvs167 centroid tracking (Figure 1F), in *vps1*Δ cells showed the same jump as in WT cells. We quantified the number of molecules of Rvs167 recruited to endocytic sites in *vps1*Δ cells (Joglekar *et al.*, 2006; Picco *et al.*, 2015) and found that it was not significantly different from that recruited to WT cells (Figure 1D). We expect that a longer invagination is likely to recruit either more molecules of Rvs167 or the same number of molecules distributed along a longer invagination. Because we observe neither higher Rvs167 molecule numbers nor larger invagination lengths, we conclude that the membrane tube is the same length as in WT. These data further suggest that the scission process is normal in *vps1*Δ cells.

We next studied invagination progression in cells lacking Rvs167. Because the Rvs complex is a dimer of Rvs161 and Rvs167 (Boeke *et al.*, 2014), deletion of the RVS167 gene effectively removes both proteins from endocytic sites (Lombardi and Riezman, 2001; Kaksonen *et al.*, 2005). We quantified the effect of *rvs167*Δ on membrane invagination (Figure 1, A, B, and E). When Sla1 was observed in *rvs167*Δ cells, nearly 30% of endocytic events displayed the beginning of movement away from the starting position—thus invagination formation—then retract back to the starting position (Figure 1, A and B). Retractions indicate failure of vesicle formation. Thus only 70% of Sla1 patches underwent apparently successful scission in *rvs167*Δ cells (Figure 1B). Similar scission rates have been measured in earlier studies (Kaksonen *et al.*, 2005; Smaczynska-de Rooij *et al.*, 2010; Kishimoto *et al.*, 2011). We classified endocytic events into successful and retracting events and analyzed the average centroid movement in these two classes. Sla1 centroid movement in both successful and retracting endocytic events in *rvs167*Δ cells looks similar to that in WT up to invagination length of about 50 nm (Figure 1E and Supplemental Figure S1E). In WT cells, Abp1 intensity begins to drop at scission time (Supplemental Figure S1B) (Picco *et al.*, 2015). Abp1 intensity in *rvs167*Δ cells dropped after Sla1 centroid moved about 50 nm, suggesting that scission occurs in successful events at invagination lengths around 50 nm (Supplemental Figure S1D). That membrane scission occurs at shorter invagination lengths than in WT is corroborated by the smaller vesicles found using CLEM in *rvs167*Δ cells (Kukulski *et al.*, 2012). CLEM has moreover shown that Rvs167 localizes to endocytic sites after the invaginations are about 50 nm long (Kukulski *et al.*, 2012). Normal initial Sla1 movement in *rvs167*Δ indicates therefore that membrane invagination is unaffected until Rvs would normally arrive.

Synaptojanins influence vesicle uncoating, but not scission dynamics

As Vps1 did not appear to influence membrane scission, we proceeded to test the potential role of synatojanins in scission (Liu *et al.*, 2009). Apart from their role in vesicle uncoating, synaptojanins have been proposed to mediate scission with their $PI(4,5)P_2$ hydrolysis activity (Sun *et al.*, 2007; Toret *et al.*, 2008). In this model, BAR domains coat the invaginated tube, and preferential hydrolysis of $PI(4,5)P_2$ at the invagination tip unprotected by BAR proteins generates line tension, eventually causing membrane scission. We reasoned that if the yeast synaptojanins are involved in scission,

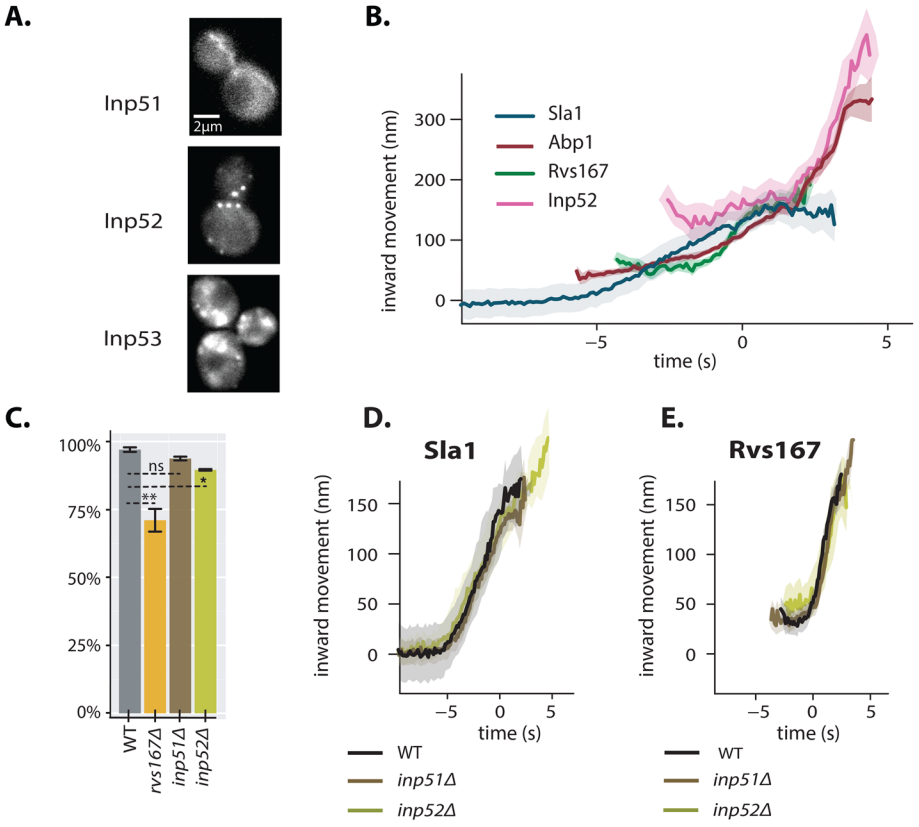

FIGURE 2: Synaptojanin-like proteins do not significantly influence endocytosis. (A) One thousand millisecond exposures from time-lapse movies of cells with endogenously tagged Inp51-, Inp52-, and Inp53-eGFP. (B) Inp52 centroid trajectory aligned in space and time to other endocytic proteins. (C) Scission efficiency in WT, *rvs167*Δ, *inp51*Δ, and *inp52*Δ cells. Error bars are SD, with *p* values from two-sided *t* test, $*p \leq 0.05$, $**p \leq 0.01$, $***p \leq 0.001$. (D) Centroid positions of Sla1-eGFP in WT, *inp51*Δ, and *inp52*Δ cells. (E) Centroid positions of Rvs167-eGFP in WT, *inp51*Δ, and *inp52*Δ cells. All centroids were coaligned with Abp1-mCherry so that time = 0 s corresponds to Abp1 intensity maximum and *y* = 0 nm corresponds to position of nonmotile Sla1 in the corresponding strains. Shading on plots represents 95% confidence interval.

their deletion should alter the invagination dynamics visualized with Sla1-eGFP or Rvs167-eGFP. Three synaptojanin-like proteins have been identified in *S. cerevisiae*: Inp51, Inp52, and Inp53. Inp51-eGFP exhibits a diffuse cytoplasmic signal, Inp52-eGFP localizes to endocytic sites, and Inp53 localizes to patches within the cytoplasm (Figure 2A) (Bensen *et al.*, 2000; Sun *et al.*, 2007). Because Inp52 can be observed at endocytic sites, we began with determining the spatial and temporal recruitment of Inp52 within the endocytic machinery. We tracked and aligned the averaged centroid of Inp52 in relation to other endocytic proteins. To do this, we imaged Inp52-eGFP simultaneously with Abp1-mCherry. We also imaged Sla1-eGFP and Rvs167-eGFP, each paired with Abp1-mCherry. Using Abp1 as the common reference frame, we were able to compare the arrivals of the different proteins with respect to that of Abp1. We assigned as time = 0 s the peak fluorescence intensity of Abp1. In WT cells, this peak is concomitant with membrane scission and also coincides with the peak Rvs167 fluorescence intensity (Supplemental Figure S1B) (Picco *et al.*, 2015). On the *y*-axis, 0 nm indicates the nonmotile position of the Sla1 centroid. Positions of the other centroids are spatially and temporally aligned to each other (Figure 2B and Supplemental Figure S2A). This analysis showed that Inp52 molecules arrived after Rvs167 and localized to the invagination tip. The localization and assembly dynamics of Inp52 are consistent with a role in the late stage of membrane invagination. Inp52 has been shown to interact with Abp1 (Stefan *et al.*, 2005). The fact that the centroid of Inp52 does not overlap with Abp1 when it arrives at endocytic sites suggests that Inp52 likely interacts with a subset of Abp1 molecules at the invagination tip.

Inp53 was not investigated further because it could not be detected at endocytic sites (Figure 2A) and is likely localized to the *trans*-Golgi network (Bensen *et al.*, 2000). Although we were unable to observe localization of Inp51 at the plasma membrane (Figure 2A), deletion of Inp51 has been shown to exacerbate the effect of *inp52*Δ on endocytosis (Singer-Krüger *et al.*, 1998), so both Inp51 and Inp52 were tested as potential scission regulators.

*inp51*Δ*inp52*Δ cells have dramatic morphological and growth defects, defects in vacuole morphology and budding polarity (Singer-Krüger *et al.*, 1998; Stolz *et al.*, 1998a). These cells also have drastically altered $PI(4,5)P_2$ levels (Stolz *et al.*, 1998b), which likely affect the assembly, disassembly, and function of many $PI(4,5)P_2$-binding endocytic proteins. The double mutation reportedly causes aberrations in endocytic coat, myosin, and actin network behavior (Sun *et al.*, 2007). Coat proteins Sla1, Sla2, and Ent1 have elongated lifetimes at endocytic sites, as does type I myosin Myo5, as well as Rvs167. Time taken for Abp1 assembly and disassembly is more than doubled (Sun *et al.*, 2007). That multiple endocytic phases, including scission, are affected in the double mutation makes it difficult to demonstrate a direct role in scission. Patches of Rvs167-eGFP tracked in these cells persist instead of disassembling immediately after inward movement, leading to aggregation of fluorescent patches inside the cytoplasm (Supplemental Figure S2C). We cannot, using the methods used here, distinguish between scission and other defects. We reasoned that a quantitative analysis of single mutants was therefore better suited to reveal a scission-specific function for synaptojanins without perturbing overall $PI(4,5)P_2$ homeostasis.

Dynamics of Sla1-eGFP and Rvs167-eGFP in *inp51*Δ and *inp52*Δ cells were compared against the WT (Figure 2, C–E). Scission efficiency did not significantly decrease in *inp51*Δ compared to the WT but showed a slight decrease in *inp52*Δ cells (Figure 2C). The movement of Sla1 and Rvs167 centroids in successful endocytic events in *inp51*Δ were virtually the same as in WT (Figure 2, D and E), while Rvs167 assembly and disassembly took longer (Supplemental Figure S2B). Rvs167 signal in *inp51*Δ cells persisted longer compared to the WT (Figure 2E), likely because of a delay in Rvs167 disassembly from the newly formed vesicle. In *inp52*Δ cells Sla1 centroid movement had the same magnitude and rate as in WT, but Sla1-eGFP signal was persistent after inward movement (Figure 2D). Rvs167 in *inp52*Δ cells appears to rebound slightly, but this movement is within the confidence interval of centroid tracking. Sla1 assembly and disassembly, as well as Rvs167 disassembly were aberrant in *inp52*Δ cells compared to WT (Supplemental Figure S2A). These data are

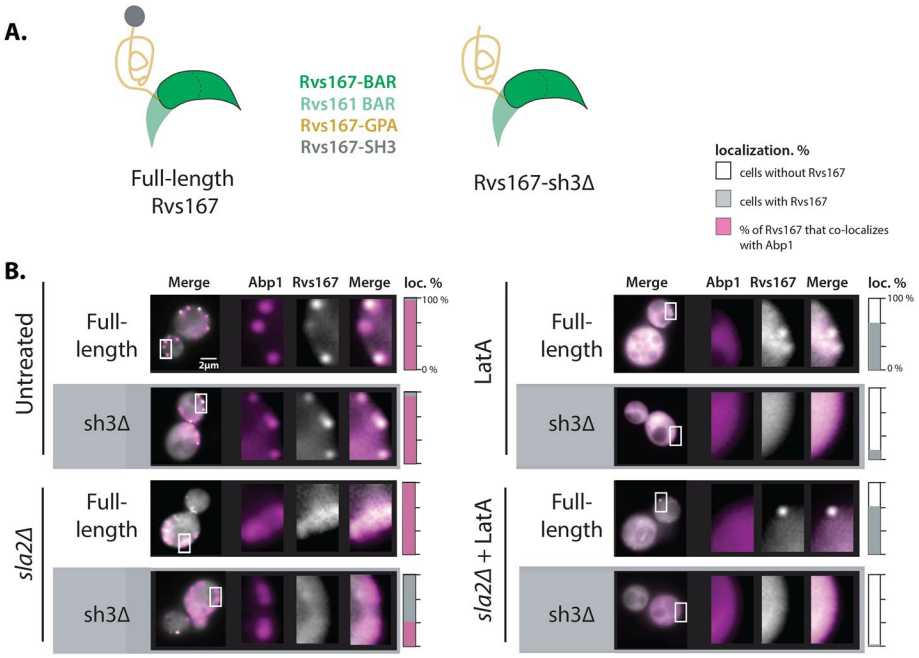

FIGURE 3: Rvs167 BAR domains need membrane curvature to localize to endocytic sites. (A) Schematic of Rvs protein complex with and without the SH3 domain. (B) One thousand millisecond exposures from time-lapse movies, showing localization of full-length Rvs167 and Rvs167-sh3Δ in WT, *sla2*Δ, LatA treated, and LatA-treated *sla2*Δ cells. Bars indicate percentage of cells with Rvs167 cortical patches and percentage of cells that contain both Rvs167 and Abp1.

consistent with synaptojanin involvement in assembly and disassembly of coat and scission proteins at endocytic sites (Toret *et al.*, 2008). However, because the centroid movements of Sla1 and Rvs167 are unaltered, synaptojanins may not have a direct or major role in membrane scission.

Rvs BAR domains likely recognize membrane curvature in vivo

So far Rvs167 and Rvs161 remain the proteins that have the most significant influence on scission efficiency. Recruitment to and interaction of the Rvs complex at endocytic sites was thus investigated further. The Rvs complex can tubulate liposomes in vitro, likely via the BAR domain (Youn *et al.*, 2010). Interaction of the BAR domain with membrane curvature in vivo has, however, not been tested. The Rvs167-SH3 domain can interact with proteins associated with actin patches such as Abp1, Las17, Myo3, Myo5, and Vrp1, but the role of these interactions in vivo is not known (Lila and Drubin, 1997; Colwill *et al.*, 1999; Madania *et al.*, 1999; Liu *et al.*, 2009). We first tested the BAR-membrane interaction by deleting the SH3 domain to remove its contribution (Figure 3A). We then observed localization of Rvs167-sh3Δ in *sla2*Δ cells. Sla2 is required for endocytic membrane invagination, and in *sla2*Δ cells only flat membrane (Picco *et al.*, 2018) or shallow invaginations (<50 nm) (Idrissi *et al.*, 2012) have been observed at endocytic sites. Sla2 acts as the molecular linker between forces exerted by the actin network and the plasma membrane (Skruzny *et al.*, 2012). *sla2*Δ cells therefore contain a polymerizing actin network at endocytic patches, but the membrane has no tubular curvature, and endocytosis fails (Skruzny *et al.*, 2012; Picco *et al.*, 2018). Colocalizations of endogenously tagged full-length Rvs167-eGFP and Rvs167-sh3Δ-eGFP with Abp1-mCherry in WT and *sla2*Δ cells were compared (Figure 3B). We thus tested whether Rvs BAR domain could be recruited to the endocytic sites in *sla2*Δ cells, independent of tubular curvature. In *sla2*Δ cells, the full-length Rvs167 colocalized with Abp1-mCherry, indicating that it was recruited to endocytic sites without tubular curvature (Figure 3B, "*sla2*Δ," and Supplemental Figure S3). Rvs167-sh3Δ did not appear at the plasma membrane except for rare transient patches. Therefore, Rvs167-sh3Δ, that is, the BAR domain alone, is recruited to endocytic sites only when tubular curvature is present. Additionally, localization of the full-length protein in *sla2*Δ cells is therefore likely via SH3 domain interaction. In this experiment, we cannot separate the direct effect of membrane curvature from the effect of curvature enriched in specific lipid types (McMahon and Boucrot, 2015). BAR domain interaction with curved membrane could therefore reflect interaction with one or the other, or a combination of both.

Rvs SH3 domains mediate actin- and membrane curvature–independent localization

We wanted to distinguish between Rvs association with membrane curvature and actin. Latrunculin A (LatA) inhibits actin polymerization and therefore the assembly of actin and actin-related proteins at endocytic sites. *sla2*Δ as well as LatA remove tubular membrane curvature, but *sla2*Δ retains actin patches at endocytic sites (Kukulski *et al.*, 2012; Picco *et al.*, 2018). To study the interaction of Rvs at endocytic sites without actin proteins, we observed the localization of Rvs167 and Rvs167-sh3Δ in LatA-treated WT cells (Figure 3B, "LatA"). We also observed full-length and mutant protein in *sla2*Δ cells treated with LatA, so that we could be sure that we removed any capacity for tubular membrane curvature, as well as actin-related proteins (Figure 3B, "*sla2*Δ + LatA"). Full-length Rvs167 localized transiently at the plasma membrane in WT cells treated with LatA as well as in *sla2*Δ cells treated with LatA (Figure 3B). Rvs167-sh3Δ did not localize to the plasma membrane in either case. Thus, localization of full-length Rvs167 in the presence of LatA in both WT and *sla2*Δ cells is due to the SH3 domain. This also indicates that the SH3 domain is able to recruit Rvs molecules to the plasma membrane in an actin- and curvature-independent manner. SH3-eGFP domains expressed alone do not localize to cortical patches (unpublished data). They are likely unstable as single domains or do not have the cellular context in the absence of the other domains to arrive at endocytic sites. The role of the SH3 domain in the recruitment of the Rvs complex is unlikely to be primary and probably enhances or stabilizes interaction between BAR domains and endocytic invaginations.

Rvs167 SH3 domains are likely recruited by Myo3

Type I myosins Myo3 and Myo5 and yeast verprolin Vrp1 have known genetic or physical interactions with the Rvs167 SH3 domain (Lila and Drubin, 1997; Colwill *et al.*, 1999; Madania *et al.*, 1999; Liu *et al.*, 2009). Syp1 is an early endocytic protein that remains at endocytic sites upon LatA treatment and contains the proline-rich sequences that are typically recognized by SH3 domains (Boettner *et al.*, 2009). Bbc1 regulates growth of the actin network, arrives during the late stages of endocytosis, and is enriched in SH3 binding

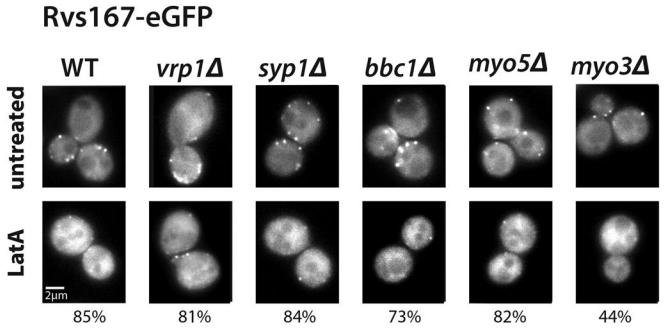

FIGURE 4: Myo3 likely recruits Rvs167 in the absence of membrane curvature. Two hundred millisecond exposures from time-lapse movies showing Rvs167-eGFP localization in untreated and LatA-treated WT, *vrp1*Δ, *syp1*Δ, *bbc1*Δ, *myo5*Δ, and *myo3*Δ cells. Percentages are averaged number from two experiments. They indicate number of LatA-treated cells in which Rvs167-eGFP is localized at the plasma membrane.

motifs (Kaksonen *et al.*, 2005; MacQuarrie *et al.*, 2019). We tested the possible role of these proteins in the SH3-dependent localization of Rvs167 in cells with the gene for one of these proteins deleted and treated with LatA (Figure 4). By using LatA we expected to reproduce the situation in which the interaction between the BAR domain and tubular membrane is removed. Then, if we lost SH3 interaction because we removed the protein with which it interacts, we would lose localization of Rvs167 completely. In *vrp1*Δ, *syp1*Δ, and *myo5*Δ cells, LatA treatment did not remove the localization of Rvs167: 81, 84, and 82% of cells, respectively, still showed Rvs167 localization, similar to WT localization. LatA treatment of *bbc1*Δ cells showed a slight decrease in Rvs167 localization compared to WT, but *myo3*Δ combined with LatA treatment reduced localization of Rvs167 most significantly: only 44% of cells showed Rvs167 localization. This indicates that SH3 domains interact at endocytic sites primarily with Myo3. Myo3 is recruited at nearly half the number as Myo5 (37.8 ± 4.0, 76.7 ± 8.1, median numbers ± SEM [Manenschijn *et al.*, 2019]), so the dramatic effect of *myo3*Δ suggests a specific preference for Myo3. Both Myo3 and Myo5 have proline-rich regions that could act as SH3 binding sites, and sequence differences between the two could contribute to preferential binding of Rvs167 to Myo3. Other proteins with proline-rich regions like Pan1 and Las17 were not investigated because the deletions are either lethal to yeast cells (Pan1) or make the cells very sick (Las17). Earlier assembly and disassembly of these proteins compared with that of Rvs167, as well as Rvs167 recruitment in Pan1-depleted cells, however, suggest that they are not likely interaction partners of Rvs167 SH3 domains (Picco *et al.*, 2015; Sun *et al.*, 2015).

Deletion of Rvs167 SH3 domain affects coat and actin dynamics

Because the Rvs167 SH3 domain had an influence on the recruitment of the Rvs complex to endocytic sites, we wondered whether the domain affects not just recruitment of the protein, but also invagination progression. We compared the dynamics of coat, actin, and scission markers in WT and *rvs167-sh3*Δ cells (Figure 5).

The Sla1 centroid position in *rvs167-sh3*Δ cells at scission time is about 70 nm from the plane of the plasma membrane, compared with 150 nm in WT, and this movement takes 8 s compared to 5 s in WT (Figure 5, A and B). The total movement of the Rvs167-sh3Δ centroid is half that of full-length Rvs167 (Figure 5, A and B). Reduced movements of both Sla1 and Rvs167-sh3Δ centroids in *rvs167-sh3*Δ cells are consistent with the formation of shorter endocytic invaginations in these cells.

We observed that Rvs167-sh3Δ recruitment begins at nearly the peak of Abp1 recruitment in *rvs167- sh3*Δ cells, while in WT, full-length Rvs167 is recruited halfway into Abp1 recruitment (Figure 5, C and D). Rvs167-sh3Δ accumulation, however, began when the Abp1 molecule number in the mutant was the same as in WT (300 copies, Figure 5, C and D). Both Rvs167 and Rvs167-sh3Δ molecules arrived at endocytic sites when the Sla1 centroid was 30–50 nm away from its starting position, so the endocytic coat has moved a certain amount when both WT and mutant forms of Rvs start to be recruited. That Rvs167-sh3Δ recruitment begins at a certain length of the invagination suggests that the Rvs complex is recruited to a specific geometry of membrane invagination. Rvs167-sh3Δ accumulation may be delayed because invaginations in these cells take longer to acquire this geometry.

We think that Rvs molecules in WT cells likely arrive below our detection threshold and that the arrival of the molecules supports invagination growth. As the invagination grows, Rvs continues to accumulate on the invagination tubes, and molecule numbers are eventually large enough to be detected. In support of this, CLEM has shown that when Rvs167 molecules are detected at endocytic sites, the invaginations are about 50 nm long, shortly after the membrane is already tubular (Kukulski *et al.*, 2012; Picco *et al.*, 2015). Because Rvs167-sh3Δ molecules accumulate more slowly than full-length protein, their support to membrane growth is less effective, and the invagination grows more slowly. Abp1 accumulation correlates with invagination growth, and slower invagination growth accumulates Abp1 more slowly. Recruitment of Rvs167-sh3Δ was significantly reduced compared to Rvs167 (Figure 5, C and D), although the cytoplasmic concentrations of the two were similar (Supplemental Figure S4). Recruitment therefore is unlikely to be limited by expression of the mutant protein. Abp1 disassembly time was increased to 15 s in *rvs167-sh3*Δ cells compared to 5 s in WT, and the total number of Abp1 molecules recruited was reduced from nearly 600 to 400, 60% of WT recruitment (Figure 5, C and D, and Supplemental Figure S5). Recruitment and disassembly defects of Abp1 indicate disruption of actin network dynamics in *rvs167-sh3*Δ cells.

In WT cells, the numbers of Rvs167 and Abp1 molecules peak at the same time. Thus, the actin network begins disassembling as soon as scission occurs (Figure 5C). However, in *rvs167-sh3*Δ cells, the numbers of Rvs167 and Abp1 molecules peaked asynchronously, with Rvs167 peaking later (Figure 5D). This observation suggests that there is a feedback mechanism between the actin network and membrane scission and that this feedback is also disrupted in *rvs167-sh3*Δ cells.

Increased BAR domain recruitment corresponds to increased membrane movement

Reduced Sla1 movement was observed in both *rvs167*Δ (Figure 1) and *rvs167-sh3*Δ (Figure 5) cells, in which about half the WT number of Rvs167 molecules are recruited (Figure 5). This suggests that increased Sla1 movement correlates with increased recruitment of Rvs167. We wondered whether Sla1 movement would scale with the amount of Rvs recruited to endocytic sites. This could suggest that recruitment of Rvs BAR domains scaffolds the membrane invagination and protects it against membrane scission (Boucrot *et al.*, 2012; Dmitrieff and Nédélec, 2015). We titrated the amount of Rvs expressed in cells by duplicating the open reading frame of RVS167 and RVS161 genes (Huber *et al.*, 2014). We also generated a strain in which the *rvs167-sh3*Δ gene was duplicated. We thus obtained cells containing either 2× copies of both RVS genes (2xRVS),

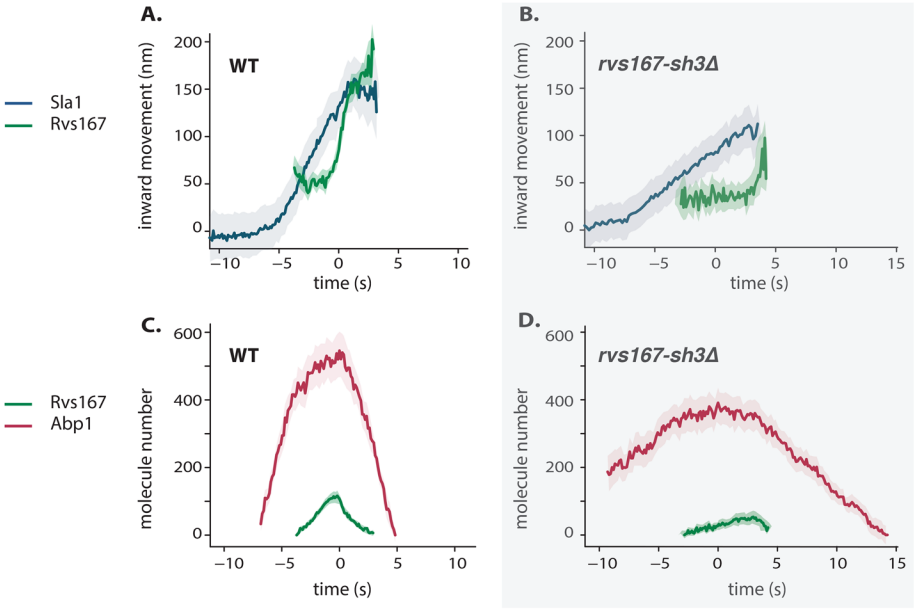

FIGURE 5: Endocytic dynamics is changed in *rvs167-sh3*Δ cells. (A, B) Centroid positions of Sla1 and Rvs167 in WT and *rvs167-sh3*Δ cells. (C, D) Numbers of molecules in WT and *rvs167-sh3*Δ cells. Centroids were aligned so that time = 0 s corresponds to Abp1 intensity maximum in the respective strains and $y = 0$ nm corresponds to nonmotile Sla1 position. Shading represents 95% confidence interval.

1× copy of the RVS genes (1xRVS, i.e., WT), 2× copies of *rvs167-sh3*Δ (2xBAR), or 1× copy of *rvs167-sh3*Δ (1xBAR) (Figure 6, A–D). In the 2xBAR strain, RVS161 was not duplicated. This is because we measured the number of molecules of mutant Rvs167 recruited in the 2xBAR strain with and without RVS161 duplicated and found that they were the same, suggesting that Rvs161 protein expression is not limiting for assembly of the Rvs complex in this strain (unpublished data). So we used the genetically simpler strain, without the RVS161 duplication.

The maximum number of WT and mutant Rvs167 molecules recruited at endocytic sites varied in 1xRVS (WT), 2xRVS, 1xBAR, and 2xBAR strains between 50 and 180 copies (Figure 6A and Supplemental Figure S6). Excess Rvs recruited in 2xRVS cells (compared to 1xRVS) did not change the total movement of the Rvs167 centroids, but Rvs disassembly took longer (Figure 6A). In the 2xBAR case, the number of Rvs167-sh3Δ molecules recruited to endocytic sites increased compared to 1xBAR, as did the movement of the centroid (Figure 6, A and B). BAR domain recruitment increased progressively from 1xBAR to 2xBAR, 1xRVS, and was finally maximal in 2xRVS cells. The trend of inward movement of the Rvs167 centroid suggests that movement correlates with the number of BAR molecules recruited to sites but saturates in the case of 2xRVS. The delayed disassembly of 2xRVS compared to 1xRVS may be due to a change in interaction between the BAR domains and underlying membrane. The membrane may be already saturated with bound RVS, causing perhaps interaction between Rvs dimers rather than Rvs and membrane. Alternatively, excess Rvs molecules may be recruited to the vesicle, so there is a delay in disassembly of these molecules compared to those on the invagination tube. Excess Rvs molecules added to the invagination tip would also account for the slight upward shift in the Rvs167 starting position in the 2xRVS strain (Figure 6B).

Abp1 molecule numbers and lifetimes at endocytic sites were different between the 1xRVS, 2xRVS, 1xBAR, and 2xBAR strains (Figure 6D and Supplemental Figure S5). The total numbers of Abp1 molecules recruited were reduced in 1xBAR compared to 2xBAR, 1xRVS, and 2xRVS (Figure 6D and Supplemental Figure S6). As Abp1 molecule numbers increased, shorter lifetimes, approaching that of WT Abp1, were observed (Supplemental Figure S5). Comparing between the 1xBAR, 2xBAR, 1xRVS (WT), and 2xRVS strains, the cells with higher Abp1 molecule numbers showed larger total movement of the Sla1 centroid (Figure 6, C and D). This indicates a correlation between the maximum number of Abp1 molecules recruited and total invagination length. In *rvs167*Δ cells, measured Abp1 molecule numbers were about the same as in WT (Figure 6D). Quantification of Abp1 molecule numbers in these cells is confounded by the existence of two types of endocytic events: successful and retracting events. We were unable to separate these events in the molecule number quantification, but we speculate that retracting events may continue to assemble an actin network during or after retraction. This accumulation could compensate for smaller Abp1 numbers that may have been measured at successful endocytic events. Much smaller percentages of endocytic events in 1BAR and 2xBAR retract, so we do not expect retracting endocytic invaginations in these cells to confound the Abp1 quantification significantly (Supplemental Figure S6). Inward movement of Sla1 in *rvs167*Δ appears closer to that in 2xBAR than to that in 1xBAR. We think the Abp1 peak in *rvs167*Δ (Figure 6D, yellow dashed line in Figure 6C) likely denotes scission, so further inward movement of Sla1 in these cells is likely movement of the vesicle post scission rather than during membrane invagination. The inward movement of Sla1 in 1xBAR cells appears similar to that in *rvs167*Δ (up to the dashed cyan and yellow lines, which indicate likely scission). We think that the 1xBAR has a deleterious effect on coat movement and results in behavior similar to that of the full deletion.

We found that, in general, increased expression of RVS caused a corresponding increase in recruitment of Rvs molecules to endocytic sites. We also found that the number of Rvs BAR domains recruited to membrane invaginations correlates positively with total length of the invagination. Furthermore, this length of the invagination also correlates positively with the number of Abp1 molecules recruited.

DISCUSSION

Recruitment and function of the Rvs complex has been studied in this work, and the applicability of several membrane scission models to yeast endocytosis has been tested. We propose that Rvs is recruited to endocytic sites via interactions between the BAR domains and invaginated membrane and also via SH3-mediated protein–protein interactions. SH3 interactions are required for efficient recruitment of Rvs. We found that assembly of Rvs at the membrane invagination delays membrane scission, allowing the invagination to grow to its full length. WT invagination growth depends on recruitment of a critical number of Rvs molecules. Both timing and recruitment efficiency of Rvs appear crucial to Rvs function.

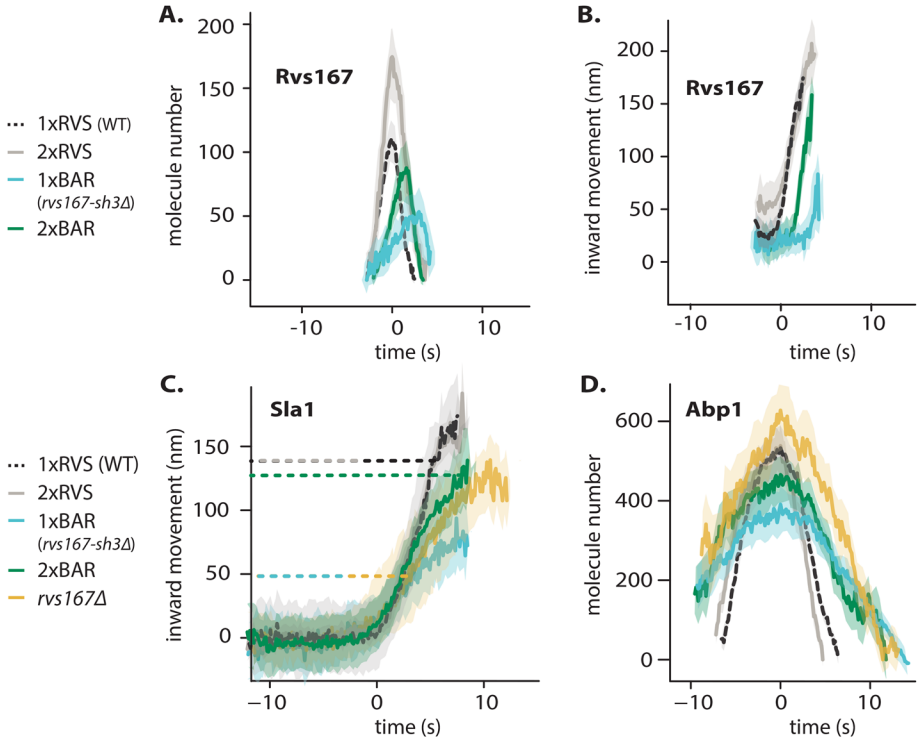

FIGURE 6: Increased BAR domain expression increases Rvs recruitment, Sla1 movement, and Abp1 recruitment. (A, B) Molecule numbers and centroid positions of Rvs167. Centroid positions were coaligned with Abp1-mCherry so that time = 0 s corresponds to Abp1 intensity maximum. (B) $y = 0$ nm is based on Sla1 positions for the respective strains. (C) Sla1 centroid positions, aligned so that the centroids begin inward movement at the same time. $y = 0$ nm corresponds to their nonmotile centroid position. Dashed lines correspond to the Sla1 centroid positions when intensity of Abp1 in the corresponding strain is at maximum. (D) Abp1 molecule number, aligned so that time = 0 s corresponds to Abp1 intensity maximum. Shading represents 95% confidence interval.

SH3 domains promote recruitment of Rvs in an actin- and membrane curvature–independent manner

Rvs167-sh3Δ accumulated to about half the number of full-length Rvs167 (Figure 5, C and D) even though similar cytoplasmic concentrations were measured for both proteins (Supplemental Figure S4), indicating that loss of the SH3 domain decreases the efficiency of recruitment of Rvs to endocytic sites. In *sla2*Δ cells, full-length Rvs167 forms patches on the membrane (Figure 3B, "*sla2*Δ"). Because Rvs167-sh3Δ does not localize to the plasma membrane in *sla2*Δ cells, localization of the full-length protein must be mediated by the SH3 domain. The full-length Rvs167 is able to assemble and disassemble at cortical patches in *sla2*Δ cells, that is, without the curvature-dependent interaction of the BAR domain (Supplemental Figure S3). This indicates that recruitment and disassembly of Rvs can occur via interactions between its SH3 domains and endocytic sites. In *sla2*Δ cells treated with LatA (Figure 3B, "*sla2*Δ+ LatA"), both tubular membrane curvature and actin are removed from endocytic sites. Full-length Rvs167 in these cells still shows transient localizations at the plasma membrane. Therefore these SH3 domains are able to localize the Rvs complex in an actin- and curvature-independent manner, and this likely acts as a secondary or parallel mechanism of localization of Rvs to endocytic sites, along with BAR-membrane interaction.

BAR domains likely recognize in vivo membrane curvature and time the recruitment of Rvs

The curved structure of endophilin and amphiphysin BAR domains allows them to interact with curved membranes. These proteins are able to form organized assemblies on tubular membranes in vitro (Mim *et al.*, 2012). Rvs167-sh3Δ localized to endocytic sites when curvature was present (Figure 3B, "Untreated"). Without the SH3 domain, and in the absence of tubular membrane curvature in *sla2*Δ cells, Rvs167-sh3Δ did not localize to endocytic sites (Figure 3B, "*sla2*Δ"). This indicates that localization of Rvs167-sh3Δ was via BAR-membrane curvature interaction. This demonstrates that Rvs BAR domains require and likely sense membrane curvature to interact with endocytic sites. Rvs167-sh3Δ had an average lifetime at endocytic sites similar to that of full-length Rvs167 (Figure 5, A and B). However, time alignment with Abp1 showed that there was a delay in the recruitment of Rvs167-sh3Δ (Figure 5, C and D). Sla1 centroid movement was slower in *rvs167-sh3*Δ cells than in WT: it takes longer for the membrane in these cells to reach the same invagination length as WT. We propose that the start of Rvs recruitment is timed to a specific membrane invagination length—therefore to a specific membrane curvature—accounting for the delay in recruitment of Rvs167-sh3Δ. The precise timing of recruitment is therefore provided by the BAR domain interacting with membrane at a specific curvature.

Recruitment of Rvs167 affects endocytic actin network dynamics

In WT cells, Abp1 and Rvs167 fluorescence intensities peaked concomitantly (Figure 5, C and D), and the consequent decays of the two coincided. Membrane scission occurs around the intensity peak of Rvs167 (Kukulski *et al.*, 2012; Picco *et al.*, 2015). Coincident disassembly therefore indicates that upon vesicle scission, the actin network is rapidly disassembled. This coincident peak was lost in *rvs167-sh3*Δ cells: Rvs167-sh3Δ fluorescence intensity peaks after Abp1 intensity starts to drop. The decay of Abp1 is also prolonged, taking over double the time as in WT. Although it is not clear what the decoupling of Abp1 and Rvs167-sh3Δ peaks means, the changes in Abp1 dynamics suggests a strong disruption of the actin network. In 1xBAR cells, the average lifetime of actin marker Abp1 was about 25 s (Supplemental Figure S5). This lifetime decreases in 2xBAR cells to about 20 s, a shift toward the WT Abp1 lifetime of around 10 s. Therefore we conclude that recruitment of the Rvs BAR domains to the invagination regulates actin network dynamics.

Rvs acts as a membrane scaffold, delaying membrane scission

Invagination length in successful endocytic events in *rvs167*Δ cells at scission time was about 50 nm (Figure 1E), only a third the WT length. Together with electron microscopy data (Kukulski *et al.*, 2012), this shows that scission can occur at much shorter

invagination lengths. In WT cells, scission does not occur at these lengths; instead invaginations grow to 150 nm (Kukulski *et al.*, 2012). Invagination lengths were increased by overexpression of the Rvs167-sh3Δ protein in 2xBAR cells compared to *rvs167*Δ and 1xBAR (Figure 6, A and C). We therefore think that localization of Rvs BAR domains to the membrane tube stabilizes the membrane and allows invaginations to progress (Boucrot *et al.*, 2012; Dmitrieff and Nédélec, 2015). Yeast endocytosis is heavily dependent on a dynamic actin network to generate the forces that bend the membrane (Kübler *et al.*, 1993; Kaksonen *et al.*, 2003; Picco *et al.*, 2018). We propose that Rvs accumulation stabilizes the membrane invagination and thereby also increases the amount of actin required to sever the membrane. This allows the invagination to grow until the WT invagination length is reached. We speculate that continued invagination growth allows the actin network to generate enough force to compensate for the stabilization. There is a limit to the stabilization by BAR domains: in 2xRVS cells, invagination lengths are the same as in 1xRVS cells even though more Rvs is recruited. It is possible that the nature of interaction of the Rvs complex with the membrane changes after a certain amount of Rvs is recruited. Once the membrane is saturated with Rvs molecules, BAR domains may interact with each other rather than with the underlying membrane. This could explain the changes in the disassembly dynamics of Rvs in the 2xRVS case (Figure 6A).

If enough forces are generated at around 50 nm, why is scission inefficient and membrane retraction rates increased in *rvs167*Δ compared to WT? Forces generated by the actin network may be at a threshold level when the invaginations are short. There could be enough force to sever the membrane, but not enough to sever reliably. The Rvs scaffold may then stabilize the membrane invagination, preventing retraction and allowing continued growth. This subsequently allows the actin network to continue growing, accumulating actin. Eventually enough actin is accumulated to reliably cause scission. We hypothesize that an increased actin amount yields greater force on the membrane. This force stretches the membrane, eventually breaking it. Controlling membrane tube length could also be a way for the cell to control the size of the vesicles formed, and therefore the amount of cargo that can be packed into the vesicle.

What causes membrane scission?

We have tested candidate proteins implicated in yeast endocytic scission and looked for scission defects. Increased Sla1 retraction rates would indicate a higher rate of scission failure. The larger total movement of Sla1 and Rvs167 centroids would indicate that a longer invagination has been formed and that scission has not occurred at normal invagination lengths. We did not see a change in Sla1 or Rvs167 centroid movements that would indicate scission defects in any other mutants that we studied, except in Rvs mutants. In *vps1*Δ cells, there is no major change in retraction rate, nor are there changes in Sla1 or Rvs167 dynamics. We conclude that Vps1 is not necessary for Rvs localization or function, and is not necessary for scission.

Sla1 and Rvs167 centroid dynamics showed that deletion of neither Inp51 nor Inp52 resulted in scission delay. In *inp51*Δ cells, Rvs167 assembly and disassembly was slightly slower than in WT: Inp51 could play a role in recruitment to and release of Rvs from endocytic sites. In the *inp52*Δ cells, about 12% of Sla1-GFP tracks retracted. Inp52 has a moderate influence on scission efficiency, but this is not apparent in our observation of invagination dynamics. In *inp52*Δ cells, Sla1 assembly is slower than in WT, and Sla1 and Rvs167 centroids persisted after scission. Inp52 likely plays a role in the assembly of coat proteins and in recycling endocytic proteins from the vesicle to the cytosolic pool. Synaptojanins could help recruit Rvs at endocytic sites via their proline-rich domains by binding Rvs167 SH3 domains. They are involved in vesicle uncoating post-scission, likely by dephosphorylating $PI(4,5)P_2$ and inducing disassembly of $PI(4,5)P_2$-binding endocytic proteins. The synaptojanins do not appear to play a major role in scission, but Inp51 and Inp52 may function synergistically to influence membrane properties. The compounded problems related to lipid hydrolysis and lack of tools that have the resolution to measure local lipid properties in vivo prevent us from conclusively ruling out line tension as a contributor to yeast endocytic scission.

Our RVS duplication data are able to test whether the protein friction model is applicable to yeast endocytic scission (Simunovic *et al.*, 2017). According to this model, a frictional force between a moving membrane tube and a coat of BAR protein bound to it causes the tube to undergo scission. Therefore, a greater frictional force should break the tube sooner than a smaller force. We increased the frictional force on the membrane by increasing the number of BAR domains bound to the membrane tube in 2xRVS cells. In 2xRVS cells, adding up to 1.6× the WT amount of Rvs at faster rates to membrane tubes did not affect the length at which the membrane undergoes scission (Figure 6). In *rvs167*Δ cells, frictional forces generated should be reduced compared to those in WT cells. Rather than increased Sla1 movement as the protein friction model would predict, we observed decreased Sla1 movement (Figure 1). We therefore think that protein friction does not contribute significantly to membrane scission in yeast endocytosis.

Similar amounts of Abp1 are recruited in both the 1xRVS and 2xRVS cases, corresponding to coat movement of about 150 nm. The magnitude of coat movement correlates with the total amount of Abp1 and, therefore, with the amount of actin recruited. A dynamic actin network is required for endocytosis in yeast (Kübler *et al.*, 1993; Picco *et al.*, 2018), and such a network is able to generate force (Theriot *et al.*, 1992). Coupling between the actin network and membrane is necessary for invagination formation (Skruzny *et al.*, 2012; Picco *et al.*, 2018). The current understanding of yeast endocytosis suggests that the membrane is pushed into the cytoplasm by an actin network polymerizing at the base of the invagination and is mechanically coupled to the invagination tip. More actin recruitment can generate greater force (Bieling *et al.*, 2016). Actin may also provide a scaffold that aids membrane invagination. More actin is therefore consistent with scaffolding as well as with increased force generation. We propose that increased Abp1 recruitment—and therefore increased actin—leads to an increasing pushing force on the membrane and that this force is responsible for invagination growth as well as for membrane scission. Stretching the membrane can eventually cause it to break, causing vesicle formation. The amount of force necessary to break the membrane is determined by properties of the membrane like rigidity and tension, by properties of the proteins accumulated on the membrane, and by the high intracellular turgor pressure in yeast cells (Dmitrieff and Nédélec, 2015). Once this force is overcome, vesicle scission occurs and membrane-bound Rvs is released. On the other hand, release of Rvs could cause instabilities in membrane shape that could also lead to scission (Dmitrieff and Nédélec, 2015). It is unclear whether scission causes release of Rvs or vice-versa. The observation that Rvs167 can accumulate and disassemble on the membrane in the absence of membrane curvature (in *sla2*Δ cells) suggests that binding–unbinding can be mediated by another interaction partner. This in turn can allow speculation that Rvs release can be triggered by this partner. A method for detecting scission with high temporal resolution is

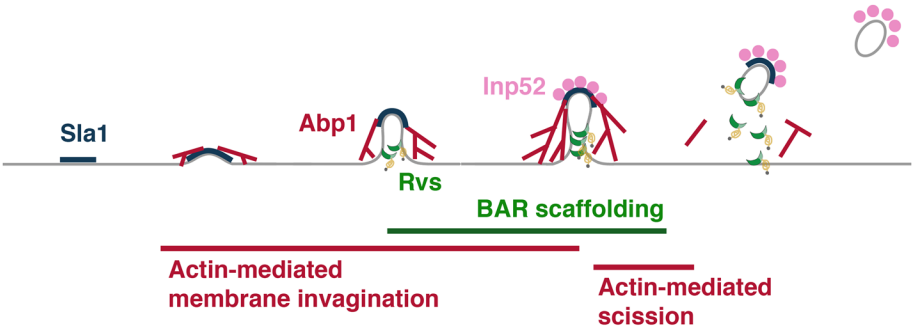

FIGURE 7: Model for yeast endocytic scission. Membrane at an endocytic site is bent by forces derived from actin polymerization. BAR domains arrive at a tubular invagination and scaffold the membrane, delaying scission. Actin forces eventually overcome the influence of BAR scaffolding, and the membrane breaks, resulting in vesicle formation.

needed to resolve whether Rvs release or scission occurs first. Release of Rvs167 SH3 domains could eventually indicate to the actin network that vesicle scission has occurred, influencing disassembly of actin components.

Our model for the late stages of endocytosis is schematized in Figure 7. We propose that Rvs is recruited to endocytic sites by two distinct mechanisms. The SH3 domain of Rvs167 recruits Rvs to endocytic sites, effectively increasing the likelihood of BAR domain interaction with tubular membrane. BAR domains bind endocytic sites by sensing tubular membrane. The membrane invagination is stabilized against scission by BAR-membrane interaction. This stabilization prevents actin-generated forces from rupturing the membrane, and the invaginations continue to grow in length as actin continues to polymerize. As actin continues to accumulate, pushing forces overcome the resistance to membrane scission. The membrane ruptures, and a vesicle is formed.

MATERIALS AND METHODS

Request a protocol through *Bio-protocol*.

Homologous recombination with PCR cassette insert

Tagging or deletion of endogenous genes was done by homologous integration of the product of a PCR using appropriate primers and a plasmid containing a selection cassette and fluorescent tag, or only selection cassette for gene deletions (Janke *et al.*, 2004). PCRs used the velocity polymerase for fluorescent tagging and Q5 for gene deletions using the NAT cassette. All fluorescently tagged genes have a C-terminus tag and are expressed endogenously. Gene deletions and fluorescent tags are checked by PCR. *vps1*Δ and gene duplications were confirmed by DNA sequencing.

Live-cell imaging

Sample preparation for live imaging. Yeast cells were grown overnight at 25°C in imaging medium synthetic complete without L-tryptophan (SC-Trp). ConA (40 µl, 4 mg/ml) was incubated on a coverslip for 10 min. Forty microliters of yeast cells at OD_{600} = 0.3–0.8 was added to the coverslip after the ConA was removed, and incubation continued for another 10 min. Non-adhered cells were then removed, adhered cells were washed 3× in SC-Trp, and 40 µl of SC-Trp was finally added to the coverslip to prevent cells from drying.

Sample preparation for live imaging in LatA-treated cells. Cells went through the same procedure as above until the last washing step. Instead of SC-Trp, 100× diluted LatA at a final concentration of 0.2 M in SC-Trp was added to the adhered cells. Cells were incubated in LatA for 10 min before imaging. For Figures 4 and 3, time-lapse movies with exposures of 200 or 1000 ms were taken using an X-CITE 120 PC (EXFO) fluorescence lamp for illumination.

Epifluorescence imaging for centroid tracking. Live-cell imaging was performed as in our previous work (Picco *et al.*, 2015). All images were obtained at room temperature using an Olympus IX81 microscope equipped with a 100×/NA 1.45 PlanApo objective, with an additional 1.6× magnification lens and a Hamamatsu ImagEM EMCCD camera. The GFP channel was imaged using a 470/22 nm bandpass excitation filter and a 520/35 nm bandpass emission filter. mCherry epifluorescence imaging was carried out using a 556/20 nm bandpass excitation filter and a 624/40 bandpass emission filter. GFP was excited using a 488 nm solid state laser, and mCherry was excited using a 561 nm solid state laser. Hardware was controlled using Metamorph software. For single-channel images, 80–120 ms was used as the exposure time. All dual-channel images were acquired using 250 ms exposure time. Dual-color images were obtained with simultaneous illumination using 488 and 561 nm lasers. A dichroic mirror and emission filters 650/75 and 525/50 were used for image acquisition and corrected using TetraSpeck beads for chromatic aberration.

Epifluorescence imaging for molecule number quantification. Images were acquired as in previous work (Picco *et al.*, 2015). Cells with fluorescently tagged protein of interest were incubated with Nuf2 cells of the same mating type, tagged with the same fluorophore. Z stacks spaced at 200 nm were acquired using 400 ms exposures on a Hamamatsu Orca-ER CCD camera. The sample was imaged with an Olympus IX81 microscope, using an X-CITE 120 PC (EXFO) fluorescence lamp for illumination.

Live-cell image analysis

EMCCD images were processed for background noise using a rolling ball radius of 90 pixels. Particle detection and tracking were performed for a particle size of six pixels, using scripts that combine background subtraction with Particle Tracker and Detector, which can be found in ImageJ (http://imagej.nih.gov). Further analysis for centroid averaging and alignments between dual-color images and single-channel images, for alignment to the reference Abp1 were done using scripts written in MATLAB (MathWorks) and R (www.r-project.org) written originally by Andrea Picco and modified for this work. Details of analysis can be found in previous work (Picco *et al.*, 2015).

Quantification of cytoplasmic concentration

From single frames of 1000 ms time-lapse images, after background subtraction and bleach correction, a circle of set radius (10 pixels) was drawn in the cytoplasm such that cortical patches are avoided. The average intensity was acquired for 10 cells of each cell type. From the same images, a circle of set radius (three pixels, whereas an endocytic patch measures about five pixels) was drawn around 10 endocytic patches from 6–10 cells of each cell type, and an average was calculated from these values.

ACKNOWLEDGMENTS

We thank the Kaksonen lab, especially Andrea Picco and Mateusz Kozak, for critical reading of the manuscript. This work was supported by the Swiss National Science Foundation (SNSF) (grant 310030B_182825) and by the National Centre of Competence in Research Chemical Biology funded by the SNSF.

REFERENCES

Bensen ES, Costaguta G, Payne GS (2000). Synthetic genetic interactions with temperature-sensitive clathrin in Saccharomyces cerevisiae. Roles for synaptojanin-like Inp53p and dynamin-related Vps1p in clathrin-dependent protein sorting at the trans-Golgi network. Genetics 154, 83–97.

Bieling P, Li T-D, Weichsel J, Huang B, Fletcher DA, Dyche Mullins R (2016). Force feedback controls motor activity and mechanical properties of self-assembling branched actin networks. Cell 164, 115–127.

Boeke D, Trautmann S, Meurer M, Wachsmuth M, Godlee C, Knop M, Kaksonen M (2014). Quantification of cytosolic interactions identifies Ede1 oligomers as key organizers of endocytosis. Mol Syst Biol 10, 756.

Boettner D, D'Agostino J, Torres O, Daugherty-Clarke K, Uygur A, Reider A, Wendland B, Lemmon S, Goode B (2009). The F-BAR domain protein Syp1 negatively regulates WASp-Arp2/3 complex activity during endocytic patch formation. Curr Biol 19, 1979–1987.

Boucrot E, Pick A, Camdere G, Liska N, Evergren E, McMahon HT, Kozlov MM (2012). Membrane fission is promoted by insertion of amphipathic helices and is restricted by crescent BAR domains. Cell 149, 124–136.

Cerveny KL, Tamura Y, Zhang Z, Jensen RE, Sesaki H (2007). Regulation of mitochondrial fusion and division. Trends Cell Biol 17, 563–569.

Cestra G, Castagnoli L, Dente L, Minenkova O, Petrelli A, Migone N, Hoffmüller U, Schneider-Mergener J, Cesareni G (1999). The SH3 domains of endophilin and amphiphysin bind to the proline-rich region of synaptojanin 1 at distinct sites that display an unconventional binding specificity. J Biol Chem 274, 32001–32007.

Colwill K, Field D, Moore L, Friesen J, Andrews B (1999). In vivo analysis of the domains of yeast Rvs167p suggests Rvs167p function is mediated through multiple protein interactions. Genetics 152, 881–893.

D'Hondt K, Heese-Peck A, Riezman H (2000). Protein and lipid requirements for endocytosis. Annu Rev Genet 34, 255–295.

Dmitrieff S, Nédélec F (2015). Membrane mechanics of endocytosis in cells with turgor. PLoS Comput Biol 11, e1004538.

Farsad K, Ringstad N, Takei K, Floyd SR, Rose K, De Camilli P (2001). Generation of high curvature membranes mediated by direct endophilin bilayer interactions. J Cell Biol 155, 193–200.

Ferguson SM, Brasnjo G, Hayashi M, Wölfel M, Collesi C, Giovedi S, Raimondi A, Gong LW, Ariel P, Paradise S, *et al*. (2007). A selective activity-dependent requirement for dynamin 1 in synaptic vesicle endocytosis. Science 316, 570–574.

Ferguson SM, Raimondi A, Paradise S, Shen H, Mesaki K, Ferguson A, Destaing O, Ko G, Takasaki J, Cremona O, *et al*. (2009). Coordinated actions of actin and BAR proteins upstream of dynamin at endocytic clathrin-coated pits. Dev Cell 17, 811–822.

Friesen H, Humphries C, Ho Y, Schub O, Colwill K, Andrews B (2006). Characterization of the yeast amphiphysins Rvs161p and Rvs167p reveals roles for the Rvs heterodimer in vivo. Mol Biol Cell 17, 1306–1321.

Galli V, Sebastian R, Moutel S, Ecard J, Perez F, Roux A (2017). Uncoupling of dynamin polymerization and GTPase activity revealed by the conformation-specific nanobody dynab. eLife 6, e25197.

Gadila SKG, Williams M, Saimani U, Delgado Cruz M, Makaraci P, Woodman S, Short JC, McDermott H, Kim K (2017). Yeast dynamin Vps1 associates with clathrin to facilitate vesicular trafficking and controls Golgi homeostasis. Eur J Cell Biol 96, 182–197.

Grabs D, Slepnev VI, Songyang Z, David C, Lynch M, Cantley LC, De Camilli P (1997). The SH3 domain of amphiphysin binds the proline-rich domain of dynamin at a single site that defines a new SH3 binding consensus sequence. J Biol Chem 272, 13419–13425.

Grigliatti TA, Hall L, Rosenbluth R, Suzuki DT (1973). Temperature-sensitive mutations in Drosophila melanogaster XIV. A selection of immobile adults. Mol Gen Genet 120, 107–114.

Gurunathan S, David D, Gerst JE (2002). Dynamin and clathrin are required for the biogenesis of a distinct class of secretory vesicles in yeast. EMBO J 21, 602–614.

Hoepfner D, van den Berg M, Philippsen P, Tabak HF, Hettema EH (2001). A role for Vps1p, actin, and the Myo2p motor in peroxisome abundance and inheritance in Saccharomyces cerevisiae. J Cell Biol 155, 979–990.

Huber F, Meurer M, Bunina D, Kats I, Maeder CI, Štefl M, Mongis C, Knop M (2014). PCR duplication: a one-step cloning-free method to generate duplicated chromosomal loci and interference-free expression reporters in yeast. PLoS One 9, e114590.

Idrissi F-Z, Blasco A, Espinal A, Geli MI (2012). Ultrastructural dynamics of proteins involved in endocytic budding. Proc Natl Acad Sci USA 109, E2587–E2594.

Janke C, Magiera MM, Rathfelder N, Taxis C, Reber S, Maekawa H, Moreno-Borchart A, Doenges G, Schwob E, Schiebel E, Knop M (2004). A versatile toolbox for PCR-based tagging of yeast genes: new fluorescent proteins, more markers and promoter substitution cassettes. Yeast 21, 947–962.

Joglekar AP, Bouck DC, Molk JN, Bloom KS, Salmon ED (2006). Molecular architecture of a kinetochore–microtubule attachment site. Nat Cell Biol 8, 581–585.

Kaksonen M, Roux A (2018). Mechanisms of clathrin-mediated endocytosis. Nat Rev Mol Cell Biol 19, 313–326.

Kaksonen M, Sun Y, Drubin DG (2003). A pathway for association of receptors, adaptors, and actin during endocytic internalization. Cell 115, 475–487.

Kaksonen M, Toret CP, Drubin DG (2005). A modular design for the clathrin- and actin-mediated endocytosis machinery. Cell 123, 305–320.

Kishimoto T, Sun Y, Buser C, Liu J, Michelot A, Drubin DG (2011). Determinants of endocytic membrane geometry, stability, and scission. Proc Natl Acad Sci USA 108, E979–E988.

Kübler E, Riezman H, Riezman H, Riezman H (1993). Actin and fimbrin are required for the internalization step of endocytosis in yeast. EMBO J 12, 2855–2862.

Kukulski W, Schorb M, Kaksonen M, Briggs JAG (2012). Plasma membrane reshaping during endocytosis is revealed by time-resolved electron tomography. Cell 150, 508–520.

Lila T, Drubin DG (1997). Evidence for physical and functional interactions among two Saccharomyces cerevisiae SH3 domain proteins, an adenylyl cyclase-associated protein and the actin cytoskeleton. Mol Biol Cell 8, 367–385.

Liu J, Sun Y, Drubin DG, Oster GF (2009). The mechanochemistry of endocytosis. PLoS Biol 7, e1000204.

Lombardi R, Riezman H (2001). Rvs161p and Rvs167p, the two yeast amphiphysin homologs, function together in vivo. J Biol Chem 276, 6016–6022.

MacQuarrie CD, Mangione MSC, Carroll R, James M, Gould KL, Sirotkin V (2019). The S. pombe adaptor protein Bbc1 regulates localization of Wsp1 and Vrp1 during endocytic actin patch assembly. J Cell Sci 132, jcs233502.

Madania A, Dumoulin P, Grava S, Kitamoto H, Scharer-Brodbeck C, Soulard A, Moreau V, Winsor B (1999). The Saccharomyces cerevisiae homologue of human Wiskott-Aldrich syndrome protein Las17p interacts with the Arp2/3 complex. Mol Biol Cell 10, 3521–3538.

Manenschijn HE, Picco A, Mund M, Rivier-Cordey AS, Ries J, Kaksonen M (2019). Type-I myosins promote actin polymerization to drive membrane bending in endocytosis. eLife 8, e44215.

McMahon HT, Boucrot E (2011). Molecular mechanism and physiological functions of clathrin-mediated endocytosis. Nat Rev Mol Cell Biol 12, 517–533.

McMahon HT, Boucrot E (2015). Membrane curvature at a glance. J Cell Sci 128, 1065–1070.

McPherson PS, Garcia EP, Slepnev VI, David C, Zhang X, Grabs D, Sossini WS, Bauerfeind R, Nemoto Y, De Camilli P (1996). A presynaptic inositol-5-phosphatase. Nature 379, 353–357.

Meinecke M, Boucrot E, Camdere G, Hon W-C, Mittal R, McMahon HT (2013). Cooperative recruitment of dynamin and BIN/amphiphysin/Rvs (BAR) domain-containing proteins leads to GTP-dependent membrane scission. J Biol Chem 288, 6651–6661.

Mim C, Cui H, Gawronski-Salerno JA, Frost A, Lyman E, Voth GA, Unger VM (2012). Structural basis of membrane bending by the N-BAR protein endophilin. Cell 149, 137–145.

Munn AL, Stevenson BJ, Geli MI, Riezman H (1995). end5, end6, and end7: mutations that cause actin delocalization and block the internalization step of endocytosis in Saccharomyces cerevisiae. Mol Biol Cell 6, 1721–1742.

Nannapaneni S, Wang D, Jain S, Schroeder B, Highfill C, Reustle L, Pittsley D, Maysent A, Moulder S, McDowell R, Kim K (2010). The yeast dynamin-like protein Vps1:vps1 mutations perturb the internalization and the motility of endocytic vesicles and endosomes via disorganization of the actin cytoskeleton. Eur J Cell Biol 89, 499–508.

Nothwehr SF, Conibear E, Stevens TH (1995). Golgi and vacuolar membrane proteins reach the vacuole in vps1 mutant yeast cells via the plasma membrane. J Cell Biol 129, 35–46.
Peter BJ, Kent HM, Mills IG, Vallis Y, Butler PJG, Evans PR, McMahon HT (2004). BAR domains as sensors of membrane curvature: the amphiphysin BAR structure. Science 303, 495–499.
Peters C, Baars TL, Bühler S, Mayer A (2004). Mutual control of membrane fission and fusion proteins. Cell 119, 667–678.
Picco A, Kukulski W, Manenschijn HE, Specht T, Briggs JAG, Kaksonen M (2018). The contributions of the actin machinery to endocytic membrane bending and vesicle formation. Mol Biol Cell 29, 1346–1358.
Picco A, Mund M, Ries J, Nédélec F, Kaksonen M (2015). Visualizing the functional architecture of the endocytic machinery. eLife 4, e04535.
Rothman JH, Howald I, Stevens TH (1989). Characterization of genes required for protein sorting and vacuolar function in the yeast Saccharomyces cerevisiae. EMBO J 8, 2057–2065.
Rothman JH, Raymond CK, Gilbert T, O'Hara PJ, Stevens TH (1990). A putative GTP binding protein homologous to interferon-inducible Mx proteins performs an essential function in yeast protein sorting. Cell 61, 1063–1074.
Rothman JH, Stevens TH (1986). Protein sorting in yeast: mutants defective in vacuole biogenesis mislocalize vacuolar proteins into the late, secretory pathway. Cell 47, 1041–1051.
Shupliakov O, Löw P, Grabs D, Gad H, Chen H, David C, Takei K, De Camilli P, Brodin L (1997). Synaptic vesicle endocytosis impaired by disruption of dynamin-SH3 domain interactions. Science 276, 259–263.
Simunovic M, Manneville J-B, Renard H-FO, Johannes L, Bassereau P, Callan A (2017). Friction mediates scission of tubular membranes scaffolded by BAR proteins. Cell 170, 172–184.
Singer-Krüger B, Nemoto Y, Daniell L, Ferro-Novick S, De Camilli P (1998). Synaptojanin family members are implicated in endocytic membrane traffic in yeast. J Cell Sci 111, 3347–3356.
Sivadon P, Crouzet M, Aigle M (1997). Functional assessment of the yeast Rvs161 and Rvs167 protein domains. FEBS Lett 417, 21–27.
Skruzny M, Brach T, Ciuffa R, Rybina S, Wachsmuth M, Kaksonen M (2012). Molecular basis for coupling the plasma membrane to the actin cytoskeleton during clathrin-mediated endocytosis. Proc Natl Acad Sci USA 109, 15092–15093.
Smaczynska-de Rooij II, Allwood EG, Aghamohammadzadeh S, Hettema EH, Goldberg MW, Ayscough KR (2010). A role for the dynamin-like protein Vps1 during endocytosis in yeast. J Cell Sci 123, 3496–3506.
Smaczynska-de Rooij II, Allwood EG, Mishra R, Booth WI, Aghamohammadzadeh S, Goldberg MW, Ayscough KR (2012). Yeast dynamin Vps1 and amphiphysin Rvs167 function together during endocytosis. Traffic 13, 317–328.
Stefan CJ, Padilla SM, Audhya A, Emr SD (2005). The phosphoinositide phosphatase Sjl2 is recruited to cortical actin patches in the control of vesicle formation and fission during endocytosis. Mol Cell Biol 25, 2910–2923.
Stolz LE, Huynh CV, Thorner J, York JD (1998a). Identification and characterization of an essential family of inositol polyphosphate 5-phosphatases (INP51, INP52 and INP53 gene products) in the yeast Saccharomyces cerevisiae. Genetics 148, 1715–1729.
Stolz LE, Kuo WJ, Longchamps J, Sekhon MK, York JD (1998b). INP51, a yeast inositol polyphosphate 5-phosphatase required for phosphatidylinositol 4,5-bisphosphate homeostasis and whose absence confers a cold-resistant phenotype. J Biol Chem 273, 11852–11861.
Sun Y, Carroll S, Kaksonen M, Toshima JY, Drubin DG (2007). PtdIns(4,5)P2 turnover is required for multiple stages during clathrin- and actin-dependent endocytic internalization. J Cell Biol 177, 355–367.
Sun Y, Leong NT, Wong T, Drubin DG (2015). A Pan1/End3/Sla1 complex links Arp2/3-mediated actin assembly to sites of clathrin-mediated endocytosis. Mol Biol Cell 26, 3841–3856.
Sweitzer SMHinshaw JE (1998). Dynamin undergoes a GTP-dependent conformational change causing vesiculation. Cell 93, 1021–1029.
Takei K, McPherson PS, Schmid SL, Camilli PD (1995). Tubular membrane invaginations coated by dynamin rings are induced by GTP-γS in nerve terminals. Nature 374, 186–190.
Theriot JA, Mitchison TJ, Tilney LG, Portnoy DA (1992). The rate of actin-based motility of intracellular Listeria monocytogenes equals the rate of actin polymerization. Nature 357, 257–260.
Toret CP, Lee L, Sekiya-Kawasaki M, Drubin DG (2008). Multiple pathways regulate endocytic coat disassembly in Saccharomyces cerevisiae for optimal downstream trafficking. Traffic 9, 848–859.
Watanabe S, Mamer LE, Raychaudhuri S, Luvsanjav D, Eisen J, Trimbuch T, Söhl-Kielczynski B, Fenske P, Milosevic I, Rosenmund C, Jorgensen EM (2018). Synaptojanin and endophilin mediate neck formation during ultrafast endocytosis. Neuron 98, 1184–1197.e6.
Youn J-Y, Friesen H, Kishimoto T, Henne WM, Kurat CF, Ye W, Ceccarelli DF, Sicheri F, Kohlwein SD, McMahon HT, Andrews BJ (2010). Dissecting BAR domain function in the yeast amphiphysins Rvs161 and Rvs167 during endocytosis. Mol Biol Cell 21, 3054–3069.
Yu X, Cai M (2004). The yeast dynamin-related GTPase Vps1p functions in the organization of the actin cytoskeleton via interaction with Sla1p. J Cell Sci 117, 3839–3853.
Zhang P, Hinshaw JE (2001). Three-dimensional reconstruction of dynamin in the constricted state. Nat Cell Biol 3, 922–926.
Zhao H, Michelot A, Koskela EV, Tkach V, Stamou D, Drubin DG, Lappalainen P (2013). Membrane-sculpting BAR domains generate stable lipid microdomains. Cell Rep 4, 1213–1223.
Zhao W-D, Hamid E, Shin W, Wen PJ, Krystofiak ES, Villarreal SA, Chiang H-C, Kachar B, Wu L-G (2016). Hemi-fused structure mediates and controls fusion and fission in live cells. Nature 534, 548–552.